

Dynamical interferences to probe short-pulse photoassociation of Rb atoms and stabilization of Rb₂ dimers

Jordi Mur-Petit, Eliane Luc-Koenig, and Françoise Masnou-Seeuws

Laboratoire Aimé Cotton, CNRS and Université Paris-Sud, Bât. 505, F-91405 Orsay, France

(Dated: March 31, 2022)

We analyze the formation of Rb₂ molecules with short photoassociation pulses applied to a cold ⁸⁵Rb sample. A pump laser pulse couples a continuum level of the ground electronic state $X^1\Sigma_g^+$ with bound levels in the $0_u^+(5S+5P_{1/2})$ and $0_u^+(5S+5P_{3/2})$ vibrational series. The nonadiabatic coupling between the two excited channels induces time-dependent beatings in the populations. We propose to take advantage of these oscillations to design further laser pulses that probe the photoassociation process via photoionization or that optimize the stabilization in deep levels of the ground state.

PACS numbers: 32.80.Qk, 33.80.Ps, 34.50.Rk

Making ultracold molecules in the lowest vibrational level $v = 0$ of the ground electronic state and creating stable molecular condensates is presently an important challenge since it opens the road toward ultracold chemistry [1, 2]. Schemes based on photoassociation (PA) of ultracold atoms [3] with cw lasers, have been very successful to form molecules in an excited electronic state. The latter have been stabilized into excited vibrational levels of the ground electronic state [4, 5], but not yet into $v = 0$ except for the case of RbCs [6]. The possibility of controlling PA by use of short laser pulses has been discussed in theoretical papers [7, 8, 9, 10] and very recently attempted by two experimental groups [11, 12], both in the rubidium case. Success in such experiments will create a bridge between the two domains of cold matter and coherent control, where femtosecond (fs) pulses are used to control chemical reactions [13]. Unfortunately, up to now, PA experiments with fs laser pulses have achieved *destruction* of the molecules already existing in the trap rather than creation of additional molecules [11, 12].

Finding ways to avoid this destructive effect is therefore a crucial step in the development of experiments. A promising route is PA through the resonant coupling mechanism as realized, with cw lasers, in Cs₂ [14] and RbCs [15]. For the case of Rb₂, it populates the $0_u^+(5S+5P_{1/2})$ and $0_u^+(5S+5P_{3/2})$ coupled series. This is a textbook example of global mixing of two molecular vibrational series due to spin-orbit (SO) coupling and manifested by strong perturbations in the Rb₂ 0_u^+ fluorescence and cw photoassociation spectra (cf. Refs. [16, 17]). The aim of the present paper is to draw attention to the *coherent* character of the time evolution in the coupled excited states *after* the PA pulse, and to the possibility or taking advantage of the subsequent dynamical interferences to optimize stabilization and avoid the destruction of the molecules. We consider a simple model with pulses in the picosecond range which populate a limited number of bound vibrational levels, and we analyze characteristic time-dependent oscillations that should appear in experimental signals.

Time-dependent fluorescence signals manifesting the coupling between deeply bound levels of the two series have been previously observed by pump-probe spec-

troscopy [18]. In this experiment, a molecular beam of Rb₂ was excited by a 120-fs laser pulse from the $v = 0$ level of $X^1\Sigma_g^+ \equiv X$ to low ($\sim 5600 \text{ cm}^{-1}$ below the $5S+5P$ asymptote) vibrational levels of the $A^1\Sigma_u^+ \equiv A$ state, with a classical inner turning point $\sim 8a_0$. A delayed pulse, operating around the outer turning point of the $b^3\Pi_u \equiv b$ potential ($12a_0$), probes the population transferred to this state. It presents an oscillatory behavior with several characteristic periods of the order of 1 ps. This is explained in terms of interferences between several paths for the motion of the wavepacket in the excited state due to the crossing, at $R_{\text{short}} \approx 9.3a_0$, of the potential energy curves (hereafter referred to as V_A and V_b), corresponding to the two Hund's case *a* A and b states.

This crossing can be seen in Fig. 1(a), where we plot V_A and V_b as determined in Ref. [19]. We also show the ground-state potential obtained by matching *ab initio* calculations [20] to the long-range dispersion potential $-\sum_n C_n/R^n$ [21], and adjusting the repulsive barrier to reproduce the large value of the scattering length [22].

In this paper, we consider PA at a detuning of $\approx 60 \text{ cm}^{-1}$ below the D₁ line ($1 \text{ cm}^{-1} \approx 30 \text{ GHz}$), exciting loosely bound vibrational levels of the coupled system in the vicinity of the up-to-now unexplored crossing at long range $R_{\text{long}} \approx 29.2a_0$ [Fig. 1(c)]. The V_A curve crosses the V_b potential curve shifted down from V_b by $\Delta E_{\text{fs}}/3 = 79 \text{ cm}^{-1}$ by the inclusion of the diagonal part of the spin-orbit effective Hamiltonian, H_{SO} [19].

The diagonalization of H_{SO} within the $\{A, \bar{b}\}$ subspace, hereafter referred to as *diabatic*, renders two Hund's case *c* $0_u^+(P_{1/2})$ and $0_u^+(P_{3/2})$ *adiabatic* curves, correlated with the $5S+5P_{1/2}$ and $5S+5P_{3/2}$ asymptotes, split by ΔE_{fs} . The mixing angle $\theta(R)$ defines the transformation from the diabatic to the adiabatic basis at a given internuclear distance R :

$$|0_u^+(P_{1/2})\rangle = \cos\theta(R) |A\rangle + \sin\theta(R) |\bar{b}\rangle, \quad (1a)$$

$$|0_u^+(P_{3/2})\rangle = -\sin\theta(R) |A\rangle + \cos\theta(R) |\bar{b}\rangle. \quad (1b)$$

In the adiabatic representation, the two excited channels are coupled by radial coupling, governed by the derivative $d\theta/dR$. We display in Fig. 1(b) the R -dependence of $\cos^2\theta$. There is a sharp variation, corresponding to a

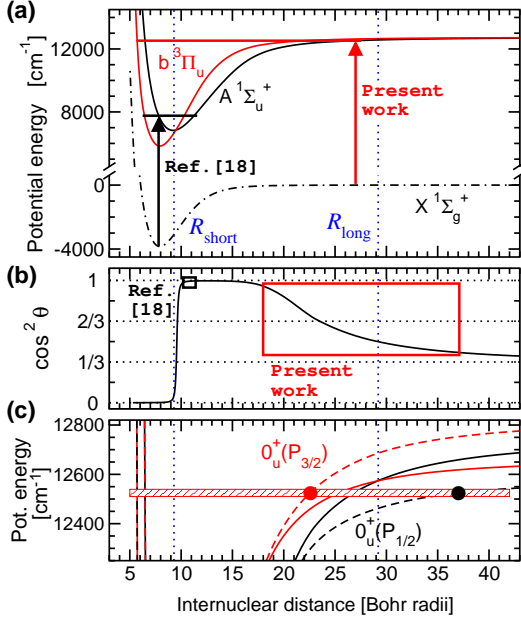


FIG. 1: (color online) (a) Potential energy curves for the ground state $X^1\Sigma_g^+$ (dash-dotted line), V_A (black, solid) and V_b [red (gray), solid]. (b) $|A\rangle$ component in $|0_u^+(P_{1/2})\rangle$ as given by Eqs. (1). (c) Zoom of the energy range where PA takes place, showing both diabatic $\{A, b\}$ (solid lines) and adiabatic (dashed) potentials. The shaded box indicates the PA window in the energy domain for the pulse studied. The dotted lines are at R_{short} and R_{long} , and symbols stand for the classical turning points of the levels contributing to the decomposition of the excited wavepacket in the uncoupled 0_u^+ basis.

singlet-triplet change of character, in the region of R_{short} , where the two diabatic curves cross abruptly. In the range of distances from $10a_0$ to $15a_0$, the splitting between the diabatic curves V_A and \bar{V}_b is very large compared to ΔE_{fs} , and $0_u^+(P_{1/2})$ has a pure singlet character. For $R > 15a_0$, $\cos^2 \theta(R)$ decreases toward its asymptotic value $1/3$, which, due to the very similar slopes of V_A and \bar{V}_b at large R [cf. Fig. 1(c)], is reached only at distances far beyond $40a_0$. In contrast with the crossing at R_{short} explored in Ref. [18], this long-range crossing is not localized.

We perform calculations for a system of ^{85}Rb atoms at a temperature of $100 \mu\text{K}$ as in the usual photoassociation experiments [11, 12]. The ^{85}Rb isotope is chosen since the manifestation of the resonant coupling between the two series is more remarkable [17]. Only s -wave scattering and $J = 0$ rotational levels are considered for simplicity, even though a full treatment of the rotational structure will be required to compare with experimental data when they become available. We consider a chirped pulse of duration τ_C , that delivers an energy E_{pulse} uniformly over an area σ . It is centered at time t_P and has a frequency that varies linearly in time, $\omega(t) = \omega_L + \chi \cdot (t - t_P)$, around the carrier frequency ω_L . The laser is red detuned from

the atomic D₁ line at ω_{D1} by $\Delta_L = \hbar(\omega_{D1} - \omega_L)$; χ is the linear chirp rate in the time domain. The instantaneous intensity $I(t)$ of the pulse involves a Gaussian envelope with a full width at half maximum equal to τ_C [23]. For this pulse, 98% of the energy E_{pulse} is delivered in the time window $[t_P - \tau_C, t_P + \tau_C]$ [8], the instantaneous laser frequency being then resonant with all the excited levels with a binding energy in the range $[\Delta_L - \hbar|\chi|\tau_C, \Delta_L + \hbar|\chi|\tau_C]$, which defines a *PA window in energy* [23], cf. Fig. 1(c).

We choose a nonperturbative description for the dynamics of the PA process and of the vibration of the molecules, and solve the time-dependent coupled Schrödinger equations [8, 9] to compute the wavepacket motion in the ground X and the excited A and b states. The X and A channels are coupled by $\hbar\Omega(t) = -\sqrt{I(t)/(2c\epsilon_0)}\mathcal{D}(R)$, where c and ϵ_0 are the speed of light and permittivity of vacuum, and $\mathcal{D}(R)$ is the molecular transition dipole moment; at large distances $\mathcal{D}(R) = 4.245ea_0$ (e = proton charge, a_0 = Bohr radius). A radial grid up to $30\,000a_0$ has been built with the mapped grid method [24] to faithfully represent the initial state as a stationary scattering level in X, and the vibrational wavefunctions in the excited states. The time propagation was performed as in Ref. [8].

From now on, we concentrate on a short PA pulse, red-detuned by $\approx 60 \text{ cm}^{-1}$ from the D₁ line (corresponding to $\lambda_{\text{pump}} = 798 \text{ nm}$). The bandwidth is set to 15 cm^{-1} , large enough to resonantly couple the initial state $|X, E = 98.85 \mu\text{K}\rangle$ with two levels of the $0_u^+(P_{3/2})$ series and 13 levels of the $0_u^+(P_{1/2})$ series, but small enough to avoid population of continuum levels in the excited state [cf. Fig. 1(c)]. The pulse is centered at $t_P = 50 \text{ ps}$, with $\tau_C = 10 \text{ ps}$, $\chi = 4.41 \times 10^{-2} \text{ ps}^{-2}$, and $E_{\text{pulse}} = 41 \text{ nJ}$ focused on $\sigma = 2.8 \times 10^{-3} \text{ cm}^2$. We choose $\chi > 0$ to maximize the population transfer [25].

We present in Fig. 2 the evolution of the population in the excited states, $|\Psi_{\text{exc}}(R, t)|^2 = |\Psi_A(R, t)|^2 + |\Psi_b(R, t)|^2$, well after the PA pulse has finished. The PA probability for a single pair of atoms is 4.21×10^{-6} , and most excited population concentrates around two peaks at $22a_0$ and $37a_0$. The relative importance of these peaks changes in time. For example, the amplitude of the peak at $22a_0$ oscillates with a period $T^* \approx 8 \text{ ps}$.

This beating results from the interferences between the population of the stationary levels v' of the coupled system of excited states. Indeed, in the present case, the coupling is such that neither the diabatic nor the adiabatic stationary vibrational levels constitute a good basis for the analysis. Here, the coupled states $|\phi_{v'}^{\text{coup}}\rangle$, which have components on the two electronic channels, are labeled by v' according to their increasing energy $E_{v'}$. In this basis, the decomposition of the two-component wavepacket reads $\Psi_{\text{exc}}(R, t) = \sum_{v'} c_{v'} \phi_{v'}^{\text{coup}}(R) \exp(-iE_{v'}t/\hbar)$, where each $c_{v'}$ as well as the total excited population are constant after the pulse.

We show in Figs. 3(b) and 3(c) the radial density $|\phi_{v'}^{\text{coup}}(R)|^2$ of two stationary states present in the ex-

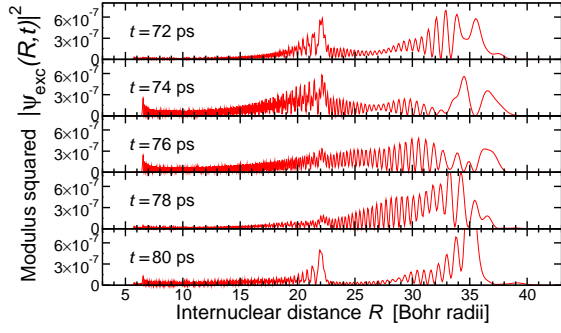


FIG. 2: (color online) Evolution of the wavepacket in the excited channels $\Psi_{\text{exc}}(R, t)$ after the PA pulse has finished.

cited wavepacket. The lower panel corresponds to a level 51 cm^{-1} below the $5S+5P_{1/2}$ limit. It turns out to be ascribable to a “ $0_u^+(P_{1/2})$ level”, as most of its probability density is accumulated close to the outer turning point $R_{\text{ext},1/2} \approx 37a_0$, corresponding to this potential and this energy [black circle in Fig. 1(c)]. The state in Fig. 3(b), which corresponds to a level 54 cm^{-1} below D_1 , is a typical example of a “resonant $0_u^+(P_{3/2})$ level” [17]: it has a 55% weight in the adiabatic $P_{3/2}$ channel, and features two maxima of probability, corresponding to the turning points $R_{\text{ext},1/2}$ and $R_{\text{ext},3/2} \approx 22a_0$ [red (gray) circle in Fig. 1(c)] in $0_u^+(P_{1/2})$ and $0_u^+(P_{3/2})$ respectively. As the instantaneous frequency of the chirped pulse is resonant with ~ 15 levels in the coupled 0_u^+ series, Ψ_{exc} will have components on stationary levels of both types, which explains the double-peak structure observed in Fig. 2.

Now, it is easy to show that the population density at an internuclear distance R has a time dependence determined by *all* the beating frequencies $\omega_{ij} = (E_i - E_j)/\hbar$, where E_i and E_j are the energies of those levels for which $c_{v'} \neq 0$. The largest weights in the decomposition correspond to the levels of the coupled basis labeled by $v' = 406$ and 408 , two “ $0_u^+(P_{1/2})$ ” levels separated by $\Delta E \approx 4.24 \text{ cm}^{-1}$, which corresponds to a beating of $T_{\text{beat}} \approx 7.85 \text{ ps}$, in agreement with T^* observed in Fig. 2.

The observed oscillation in the population density close to $R_{\text{ext},3/2}$ can be probed experimentally with a suitable laser pulse that ionizes the molecule and coherently populates several levels of the lowest $\text{Rb}_2^+(\text{X}^2\Sigma_g^+)$ potential [26] with classical turning point $R_{\text{ext},+} \approx 22a_0$. The stationary wavefunction of one such level is plotted in Fig. 3(a). Assuming that the ionization process is a vertical transition, the population transfer to the ionic channel will concern the part of the wavepacket that is close to $R_{\text{ext},+}$, *i.e.*, the peak around $R_{\text{ext},3/2}$. Indeed, we show in Fig. 4(a) the time evolution of the overlap $\sum_{v''} |\langle \text{Rb}_2^+(\text{X}^2\Sigma_g^+), v'' | \Psi_{\text{exc}}(t) \rangle|^2$ for the levels $v'' \in [185, 194]$ that have $R_{\text{ext},+} \approx (21 - 23)a_0$ and can be populated using a laser with central wavelength $\lambda_{\text{probe}} = 479.8 \text{ nm}$ and bandwidth $\approx 30 \text{ cm}^{-1}$. (The overlap is calculated with both A and b components of the excited wavepacket, as no selection rules apply to the ion-

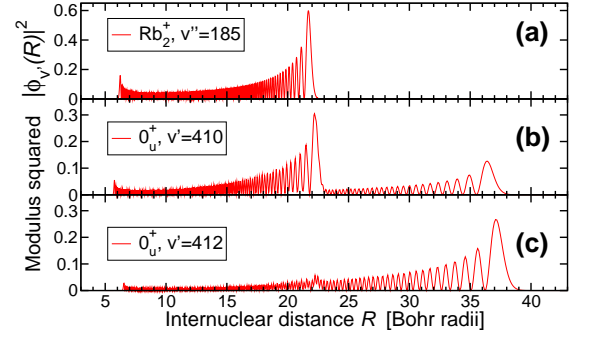


FIG. 3: (color online) Stationary wavefunctions of (a) the $\text{Rb}_2^+(\text{X}^2\Sigma_g^+)$ level bound by 264 cm^{-1} ; (b) the 0_u^+ level 54 cm^{-1} below D_1 ; and (c) the 0_u^+ level 51 cm^{-1} below D_1 .

izing transition.) The signal has a rich structure of peaks and troughs. In the Fourier transform (FT) of a longer-duration signal [cf. Fig. 4(c)], one observes a characteristic time $T_1 = 6.2 \text{ ps}$ (and its multiples), which is identified with the beating period between the levels $v' = 407$ [a “ $0_u^+(P_{1/2})$ ” level] and $v' = 410$ [a “resonant $0_u^+(P_{3/2})$ ” level, cf. Fig. 3(b)]. Thus, T_1 is a characteristic time of the $P_{1/2}$ - $P_{3/2}$ population transfer. Quite remarkably, a different ionizing pulse designed to probe the wavepacket close to $37a_0$ ($\lambda_{\text{probe}} = 469.3 \text{ nm}$) would render a signal dominated by $T_2 = 2T_{\text{beat}} = 15 \text{ ps}$, the beating period between the two “ $0_u^+(P_{1/2})$ ” levels $v' = 407, 408$ [cf. Fig. 4(b) and 4(c)]: as the classical turning point of the $0_u^+(P_{3/2})$ components is $22a_0$, where the Rb_2^+ vibrational wavefunctions have no appreciable amplitude, almost no effect of the $0_u^+(P_{1/2})$ - $0_u^+(P_{3/2})$ coupling is expected to show up at this distance. Of course, some peaks are visible in Fig. 4(c) that correspond to other beating periods ω_{ij}^{-1} . Nevertheless, T_1 and T_2 can be used as fingerprints of the two different ionization processes, as each of them appears only in one signal.

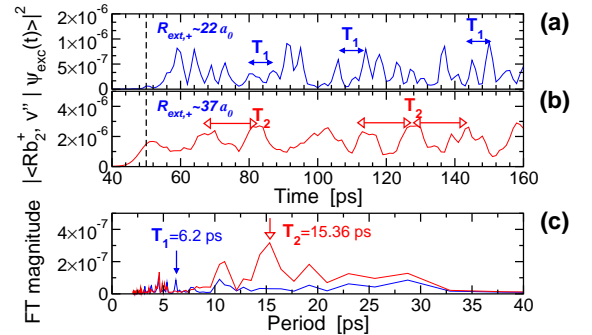


FIG. 4: (color online) Evolution of the overlap of $|\Psi_{\text{exc}}(t)\rangle$ with (a) 10 $\text{Rb}_2^+(\text{X}^2\Sigma_g^+)$ levels with $R_{\text{ext},+} \approx 22a_0$; (b) 16 $\text{Rb}_2^+(\text{X}^2\Sigma_g^+)$ levels with $R_{\text{ext},+} \approx 37a_0$. (c) Fourier transform of signals in (a) [blue (black) line] and (b) [red (gray) line] in the time window $t \in [70, 300] \text{ ps}$. The dashed vertical line stands for $t_P = 50 \text{ ps}$ and arrows indicate the most relevant timescales.

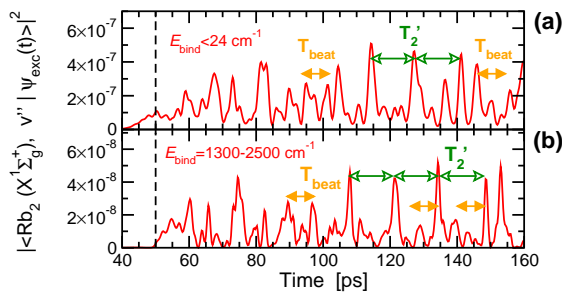


FIG. 5: (color online) Evolution of the overlap of $|\Psi_{\text{exc}}(t)\rangle$ with (a) 17 $\text{Rb}_2(X^1\Sigma_g^+)$ levels with $E_{\text{bind}} \lesssim 24 \text{ cm}^{-1}$; (b) 28 $\text{Rb}_2(X^1\Sigma_g^+)$ levels with $E_{\text{bind}} \approx 1300 - 2500 \text{ cm}^{-1}$.

We next analyze the dynamics after a dump pulse toward bound vibrational levels of $\text{Rb}_2(X^1\Sigma_g^+)$. Note that due to selection rules, this transition is selecting the $A^1\Sigma_u^+$ component in the excited wavepacket. The results are shown in Fig. 5(a) for the vibrational levels with binding energy $E_{\text{bind}} \lesssim 24 \text{ cm}^{-1}$, and in Fig. 5(b) for the levels with $1300 \text{ cm}^{-1} \leq E_{\text{bind}} \leq 2500 \text{ cm}^{-1}$, which have a reasonable Franck-Condon factor with Ψ_{exc} and are reachable by a fs dump pulse ($\lambda_{\text{dump}} = 708 \text{ nm}$). In both cases, T_{beat} and the mean value of the vibrational period in the pure $0_u^+(P_{1/2})$ potential *in this energy range*, $T'_2 \approx 13 \text{ ps}$, have an important role, and can be used to determine the best timing for the dump pulse.

In summary, we have studied the dynamics of $\text{Rb}_2 0_u^+$ molecules created by a picosecond PA pulse from cold ^{85}Rb atoms. The excited wavepacket spans ~ 15 vibrational levels in the coupled 0_u^+ basis and presents two maxima of probability at $R_{\text{ext},1/2}$ and $R_{\text{ext},3/2}$. The subsequent dynamics shows quantum interferences, with a beating of the population close to $R_{\text{ext},3/2}$. This beat-

ing can be monitored by photoionizing the wavepacket with a laser with well-defined energy spectrum, which in practice defines a window of internuclear distances whose density probability is probed. The corresponding signal and its Fourier transform can serve as identification tool for ongoing PA experiments [11, 12]. We have also analyzed a pump-dump pair of pulses to form deeply-bound ground-state molecules. The resulting time dependence would allow, in an experiment with a sequence of pump-dump pairs at a high repetition rate, to choose the delay between consecutive pairs, so that a pump pulse would not dissociate the molecules created by the preceding dump pulse. Moreover, these molecules could be further transferred to even deeper levels by other pairs of pulses (see also Ref. [10]). We studied here a pulse with a relatively large detuning to avoid coupling to the continuum levels in the excited channels. In the future, for a closer comparison with experiments, femtosecond PA pulses with smaller detunings and a mask to cut the blue part of the pulse spectrum that transfers populations to the continuum, will be analyzed. Also, we will further study the role of SO coupling in ^{87}Rb and ^{133}Cs samples.

We thank T. Bergeman, M. Aymar, and S. Azizi for providing us the potentials in Refs. [19] and [20, 26], respectively. Fruitful discussions with C. Koch, E. Dimova, O. Dulieu, R. Kosloff, A. Montmayrant, L. Pruvost, I. Walmsley, and M. Weidemüller are also gratefully acknowledged. This work was partially supported by the EC Research Training Network “Cold Molecules” (contract no. HPRN-CT-2002-00290). Laboratoire Aimé Cotton is UPR 3321 of CNRS, associée à l’Université Paris-Sud, member of Fédération Lumière Matière (FR 2764) and of Institut Francilien de Recherche sur les Atomes Froids (IFRAF).

-
- [1] D. J. Heinzen *et al.*, Phys. Rev. Lett. **84**, 5029 (2000).
 - [2] N. Balakrishnan and A. Dalgarno, Chem. Phys. Lett. **341**, 652 (2001).
 - [3] K. M. Jones *et al.*, Rev. Mod. Phys. **78**, 483 (2006).
 - [4] A. Fioretti *et al.*, Phys. Rev. Lett. **80**, 4402 (1998).
 - [5] C. Gabbanini *et al.*, Phys. Rev. Lett. **84**, 2814 (2000).
 - [6] J. M. Sage *et al.*, Phys. Rev. Lett. **94**, 203001 (2005).
 - [7] J. Vala *et al.*, Phys. Rev. A **63**, 013412 (2000).
 - [8] E. Luc-Koenig *et al.*, Phys. Rev. A **70**, 033414 (2004).
 - [9] C. P. Koch, E. Luc-Koenig, and F. Masnou-Seeuws, Phys. Rev. A **73**, 033408 (2006).
 - [10] E. A. Shapiro *et al.*, Phys. Rev. A **75**, 013405 (2007).
 - [11] B. L. Brown, A. J. Dicks, and I. A. Walmsley, Phys. Rev. Lett. **96**, 173002 (2006).
 - [12] W. Salzmann *et al.*, Phys. Rev. A **73**, 023414 (2006).
 - [13] H. Rabitz, R. de Vivie-Riedle, M. Motzkus, and K. Kompa, Science **288**, 824 (2000).
 - [14] C. M. Dion *et al.*, Phys. Rev. Lett. **86**, 2253 (2001).
 - [15] A. J. Kerman *et al.*, Phys. Rev. Lett. **92**, 153001 (2004).
 - [16] C. Amiot, O. Dulieu, and J. Vergès, Phys. Rev. Lett. **83**, 2316 (1999); H. Jelassi, B. Viarès de Lesegno, and L. Pruvost, Phys. Rev. A **74**, 012510 (2006).
 - [17] V. Kokouline, O. Dulieu, and F. Masnou-Seeuws, Phys. Rev. A **62**, 022504 (2000).
 - [18] B. Zhang, N. Gador, and T. Hansson, Phys. Rev. Lett. **91**, 173006 (2003).
 - [19] T. Bergeman *et al.*, J. Phys. B: Atom. Mol. Opt. Phys. **39**, S813 (2006).
 - [20] M. Aymar and O. Dulieu (2006), private communication.
 - [21] A. Marte *et al.*, Phys. Rev. Lett. **89**, 283202 (2002).
 - [22] E. G. M. van Kempen *et al.*, Phys. Rev. Lett. **88**, 093201 (2002).
 - [23] E. Luc-Koenig, M. Vatasescu, and F. Masnou-Seeuws, Eur. Phys. J. D **31**, 239 (2004).
 - [24] K. Willner, O. Dulieu, and F. Masnou-Seeuws, J. Chem. Phys. **120**, 548 (2004).
 - [25] C. P. Koch, R. Kosloff, and F. Masnou-Seeuws, Phys. Rev. A **73**, 043409 (2006).
 - [26] M. Aymar, S. Azizi, and O. Dulieu, J. Phys. B: Atom. Mol. Opt. Phys. **36**, 4799 (2003).